Efficient Dust Detection based on Spectral and Thermal Observations of MODIS Imagery

Hazhir Bahrami[a], Saied Homayouni[b], Reza Shah-Hosseini[a,*], Arash ZandKarimi[c], Abdolreza Safari[a]

[a] University of Tehran, School of Surveying and Geospatial Engineering, Department of Photogrammetry and Remote Sensing, Tehran, Iran

[b] Centre Eau Terre Environnement, Institut National de la Recherche Scientifique, Québec, Canada

[c] Department of Remote Sensing and GIS, Tabriz University, Tabriz, Iran

Abstract. The dust storm is one of the severe natural disasters that has been recently threatening the Middle East region due to climate changes and human activities. This phenomenon has become a national crisis in some countries in this region over the previous years, especially in spring and summer. This research aims to detect and monitor the areas covered by the seasonal and occasional dust storm from MODIS (Moderate Resolution Imaging Spectroradiometer) satellite imagery. MODIS imagery possesses impressive spectral and temporal characteristics that are essential for such an environmental application of Earth observations. An efficient algorithm, based on the spectral and statistical analysis of both thermal and reflectance bands of MODIS data, was developed through a decision tree method. To this end, an index was proposed to detect the dusts over the land using the brightness temperature of thermal bands. The results of the proposed algorithm were assessed utilizing ground-based observation of synoptic stations. The proposed method showed high reliability and performance, as well as the automatic capability of dust detection in land and sea areas of the image simultaneously. The evaluation of results showed that the proposed algorithm could detect thin and thick dust storms with an overall accuracy of about 80%. Moreover, the dust monitoring results visually agreed well with the Ozone Monitoring Instrument Aerosol Index (OMI-AI) dust products.

Keywords: Dust detection and monitoring, Brightness Temperature, MODIS Satellite Images, Middle East, OMI-AI.

***** Reza Shah-Hosseini**,** E-mail: rshahosseini@ut.ac.ir

1 Introduction

Dust storms are one of the most hazardous environmental phenomena that frequently take place in arid and semi-arid regions [1, 2]. A dust storm is the consequence of particles or sand dust picked by stormy winds from the surface of the desert. These solid particles are suspended in the air and reduce the visibility to near-zero in nearby regions [3, 4]. According to the World Meteorological Organization (WMO), the dust particles affect the cloud droplets and crystals, thus affecting the location and amount of precipitation. Therefore, the effects of dust on drought and the environment and climate change must be carefully assessed [5].

Suspended particles can cause environmental, economic, and social problems. In other words, air pollution affects people’s health, quality of agricultural products, soil fertility, and infrastructures [6, 7]. Various reports have also shown that dust storms seem to impact the quality of communications [4, 8, 9, 10, 11, 12]. Besides that, they can create irrecoverable health issues for children and people having breathing disorders [4, 13, 14].

Various factors, including atmospheric interactions, severe winds, bare soil, and lack of vegetation cover, geological structures, little rain, decreasing soil moisture, and arid climate, create such storms [15, 2, 16, 17]. These particles may rise into a higher level of the troposphere after released, and come down in the other urban or agriculture areas [18]. Consequently, real-time and automatic monitoring of dust particles is primordial for the population health [19, 6].

There are various technologies for monitoring dust storms, including ground-based observations, video surveillance, wireless sensors, satellite remote sensing [20]. The ground-based observations are among the most accurate technologies; nevertheless, they are unable to monitor the displacement of dust on a large-scale. The properties of dust particles are frequently measured by ground measurements using sun photometers [5]. The AERONET (AErosol RObotic NETwork) is a network of ground-based sun photometers that provide high temporal resolution Aerosol Optical Depth (AOD) measurements [21].

Compared to the other methods, remote sensing is recognized as the best approach for assessing the process of dust from the beginning, and over the space and time. Besides, satellite imagery can be efficient in studying how the meteorological parameters such as wind speed, wind direction, atmospheric pressure, and surface temperature affect the rise and distribution of dust in time and space [22, 23, 24]. Dust can be detected in the ultraviolet range by absorption (0.315 – 0.4 µm), in the visible spectrum by scattering and in the thermal infrared region by the difference of ground surface/aerosol emissivity [25, 26, 5, 27, 28].

Several studies have been carried out for dust detection using satellite sensors such as MODIS [25, 29, 30], NOAA-Advanced High-Resolution Radiometer (AVHRR) [31, 32], Ozone Monitoring Instrument (OMI) and Total Ozone Mapping Spectrometer (TOMS) [33, 34, 23, 35] and Cloud-Aerosol Lidar and Infrared Pathfinder Satellite Observation (CALIPSO) [36]. MODIS sensor has been significantly utilized in dust detection because of its high spectral and temporal resolution and extensive ground coverage [37, 38].

By considering the surface background, various algorithms have been developed, e.g., Dark Target for detecting dust on the sea surface [39] and Deep Blue for bright surfaces such as deserts [40, 41, 42]. Moreover, a variety of approaches based on different parts of the electromagnetic spectrum are proposed, including, thermal-based bands [43, 44, 45, 46, 47, 48, 49], visible- and near infrared-based bands [50, 51], and combination of visible and infrared spectral bands [52, 53, 25, 54, 55, 10]. Many studies focused on the temporal and spatial variability of dust aerosol frequency [33], while others concentrate on identifying dust source regions [56].

Some researches declared that the Middle East is one of the principal sources of dust in the world [57]. The primary source of these dust storms is originated from Iraq, Kuwait, Saudi Arabia, and Syria [47]. In recent years, the recurrence of dust storms in this region has been increased [58, 17]. The Shamal winds often spur dust storms in the Middle East region. Hot and dry north-westerly winds blowing across the Persian Gulf frequently in summer (in June and July), but can happen any time of year. The occurrence of the dust storms in Iran, north eastern Iraq, and Syria, the Persian Gulf, and the southern Arabian Peninsula is frequently in the summer. However, in western Iraq and Syria, the northern Arabian Peninsula is usually in the spring [59].

Numerous research works have investigated the dust storms in this region; however, most of them have several general limitations. First, some of these algorithms are not capable of distinguishing between dust and desert due to their similar spectral behavior [43, 44, 18]. Second, they have trouble discriminating between dust and clouds and dark and bright surfaces [47, 43, 44, 50, 18, 46]. Finally, most of them are not able to detect thin dust over water [43].

This paper aims to propose a method that overcomes the limitation of the previous approaches by using a combination of the visible and infrared spectra. This method is based on the spectral and statistical analysis of thermal and spectral observations to discriminate dust from other phenomena and can detect dust over both land and water areas. This method consists of four main steps as follows: i) masking clouds using reflective and thermal bands ii) detecting water bodies iii) detecting dust over lands based on an efficient index using thermal bands, and finally, iv) detecting thin dust over the water.

2. Materials and Method

2.1. Study Area

The study area is consisting of the western part of the Middle East, which includes the west and southwest of Iran, Iraq, Saudi Arabia, Kuwait, Yemen, and the United Arab Emirates (see Fig. 1). Most of these regions are located in the semi-arid and arid region and have a little annual rainfall. There are many deserts in this area. Due to Shamal winds, the areas mentioned above are typically experiencing dust in the spring and summer.

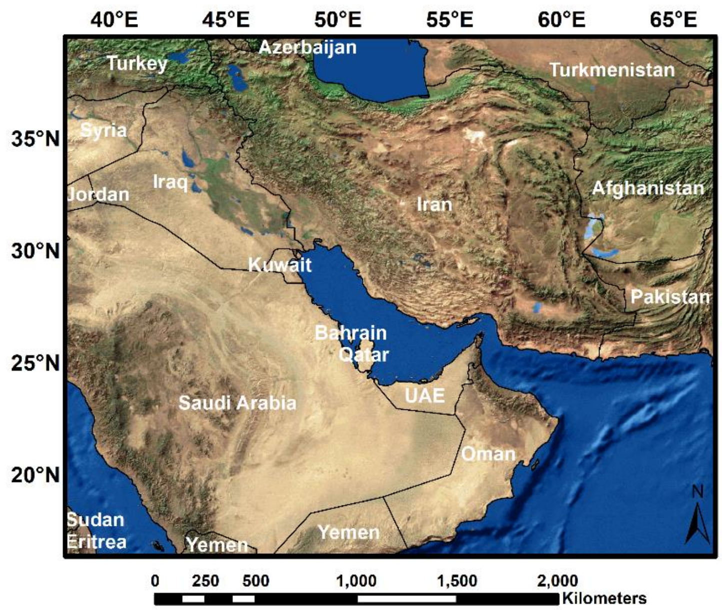

Fig. 1 The study area, the Middle East region around the Persian Gulf.

2.2. Earth Observations

2.2.1. MODIS Data

MODIS is a passive satellite sensor that provides data in the visible and infrared spectral domain, including thermal infrared. Thermal bands of MODIS sensor, installed on Aqua and Terra satellites launched in 1999 and 2002, is widely used for detecting dust in satellite images [55, 26]. MODIS has 36 bands in the visible to thermal infrared spectrum (0.4 – 14.4 µm). From these bands, bands 1 and 2 have a 250-meter resolution, while bands 3 to 7 have 500-meter resolution, and bands 8 to 36 have 1 km of resolution [25]. Thermal bands have a spatial resolution of 1 km by 1 km. These sensors are observing the entire surface of the planet Earth every day or two. Due to its extensive spatial coverage and high temporal resolution, MODIS data are useful to track large-scale phenomena and environmental changes.

In this study, we used MODIS level 1B images from both Aqua and Terra satellites. Daily MODIS Level 1B calibrated radiance data of MODIS sensors with 1 Km resolution are available through the NASA website, i.e., at http://ladsweb.nascom.nasa.gov/. Level1 B MODIS data are calibrated, geo-referenced, and geometrically corrected [60]. Re-projection and resampling were applied to the data using the MODIS conversion toolkit (MCTK). Moreover, Level 1B images were converted to brightness temperature using the MCTK toolkit. A list of the bands used for dust detection is presented in Table 1.

Table 1 List of the MODIS bands used in this study.

Band's number	Wavelength (µm)	Resolution (m)
1	0.620 – 0.670	250
2	0.841 – 0.876	250
3	0.459 – 0.479	500
4	0.545 – 0.565	500
5	1.230 – 1.250	500
7	2.105 – 2.155	500
20	3.660 - 3.840	1000
23	4.020 - 4.080	1000
31	10.780 - 11.280	1000
32	11.770 - 12.270	1000

In this study, ten MODIS images from 2008 to 2018 were used to test and evaluate the proposed dust detection algorithm. Table 2 presents a summary of these images. Three of these dust events/images were used for sample data collection and threshold estimation, while the remaining data were used to evaluate the proposed algorithm.

Table 2 Summary of dust event case studies and MODIS images used in this study.

Date	Satellite	Product
October 29, 2017	Terra	MOD021KM
July 05, 2009	Aqua	MYD021KM
May 12, 2018	Terra	MOD021KM
October 31, 2017	Aqua	MYD021KM
October 31, 2017	Terra	MOD021KM
June 19, 2012	Aqua	MYD021KM
June 19, 2012	Terra	MOD021KM
March 05, 2010	Terra	MOD021KM
June 03, 2011	Aqua	MYD021KM
June 07, 2008	Aqua	MYD021KM

2.2.2. OMI Data

OMI is a nadir-viewing near-ultraviolet (UV) and visible charge-coupled device (CCD) spectrometer aboard NASA's Aura spacecraft with a resolution of 13 km by 24 km at nadir [61]. Aura was launched on July 15, 2004. The OMI observes the Earth's surface through two UV bands, UV1 (270–314 nm) and UV2 (306–380 nm), and one visible band, VIS (350–500 nm). It is essential to mention that the time difference between Aqua's MODIS data and OMI was less than 15 min [62].

The OMI can distinguish between different aerosol types, such as dust and smoke. It can measure cloud pressure and coverage that can provide data to derive tropospheric ozone. Considering the Lambert Equivalent Reflectivity (LER) assumption, the difference between the measured and calculated radiance is described as the Aerosol Index [63]. The OMI near-UV aerosol algorithm calculates the LER at 388 nm (i.e., R^{*}_{388}) by assuming the atmosphere scattering is purely Rayleigh [64]. Calculation of the UV Aerosol Index (UVAI) as follows:

$$\mathrm{UVAI} = -100\log_{10}\left[\frac{I_{354}^{\mathrm{obs}}}{I_{354}^{\mathrm{calc}}(R^{*}_{354})}\right] \quad (1)$$

where I_{354}^{obs} is the radiation recorded by sensor and I_{354}^{calc} is calculated by assuming LER of R_{354}^{*}.

Positive UVAI values indicate absorbing aerosol (carbonaceous aerosols, desert dust, volcanic, etc.), While Negative values indicate non-absorbing aerosol. Near-zero values of UVAI also indicate clouds, minimal aerosol, or other non-aerosol [64].

In this study, OMI-Aura_L3-OMAERUV daily data was used for visual evaluation of the dust detection model.

2.2.3. Ground Observations

For performance evaluation of the proposed algorithm, the ground observations obtained from 212 synoptic stations, managed by Iran's Meteorological Organization (IMO), which observe several weather parameters every hour. These weather parameters were horizontal visibility and code 06. Code 06 is a ground observation that measures the extensive and suspended dust particles, which is not raised by the wind at or near the station at the time of observation. The remnants of dust particles that came close to the observatory station due to sandstorms of trans-local origin and reduced vertical visibility are also reported in Code 6. Due to the limited access to the synoptic data from other countries, in this study, we used only the synoptic data of the IMO. It worths mentioning that we used synoptic data at and near the time of satellite overpasses. Fig. 2 shows the distribution of these synoptic stations across the whole country.

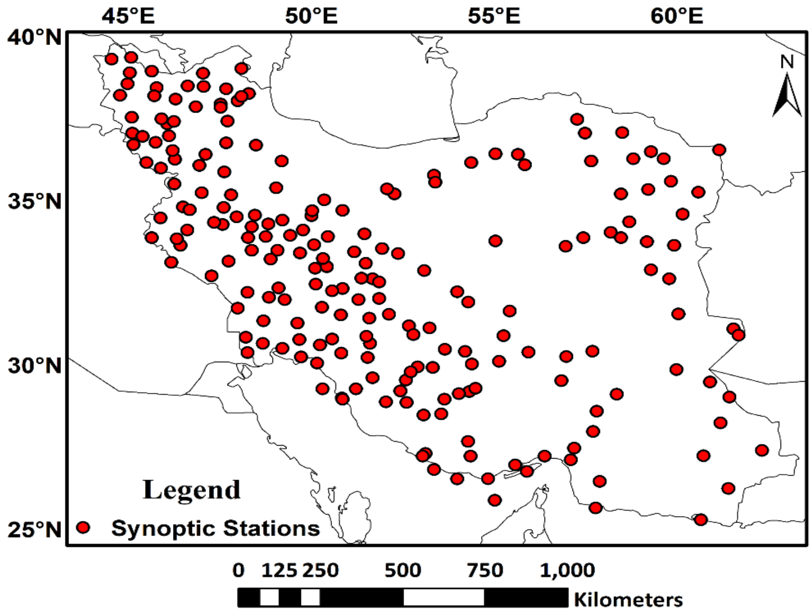

Fig. 2 The distribution of 212 synoptic stations utilized in this study.

2.3. Proposed Methodology

In this study, different steps were followed to identify the dust pixels from MODIS imagery. Statistical analysis was first performed to find suitable bands and proper thresholds for better dust detection. This analysis was based on the sampling of diverse objects (cloud, land, water, and dust over different surfaces) in the MODIS images. Training data was used to extract the relevant formula and thresholds. Three of the dust storms that occurred in 2012/06/19 (Aqua), 2011/06/03, and 2010/03/05 are considered in this study to collect training data. After sampling and finding the appropriate bands, the clouds were masked from the image. The next step was to identify water bodies. Finally, using two separate methods, the dust was detected over water and land. The flowchart of the proposed approach is shown in Fig. 3.

To implement the proposed algorithm, we need to calculate the brightness temperature of thermal bands. The brightness temperature is the temperature of a blackbody that emits the same intensity when viewed with the same detector. The amount of radiation emitted by a black body depends on its temperature, and is defined by Planck's Law:

$$B(\lambda, T) = \frac{2hc^2\lambda^{-5}}{\exp\left(\frac{hc}{kT\lambda}\right) - 1} \tag{2}$$

where B(λ,T) is the Planck function at wavelength λ(m), T is brightness temperature, $c=2.99\times10^{8}$ $m\ s^{-1}$ is the speed of light, $h=6.626\times10^{-34}$ $m^{2}\ kg\ s^{-1}$ is the Planck's constant, and $k=1.38\times10^{-23}$ $J\ K^{-1}$ is the Boltzmann's constant. Using this equation, the temperature can be derived as follows:

$$T = \frac{hc}{\lambda k \ln\left(1 + \frac{2hc^2}{L\lambda^5}\right)} \tag{3}$$

where L is the radiance value for a given pixel.

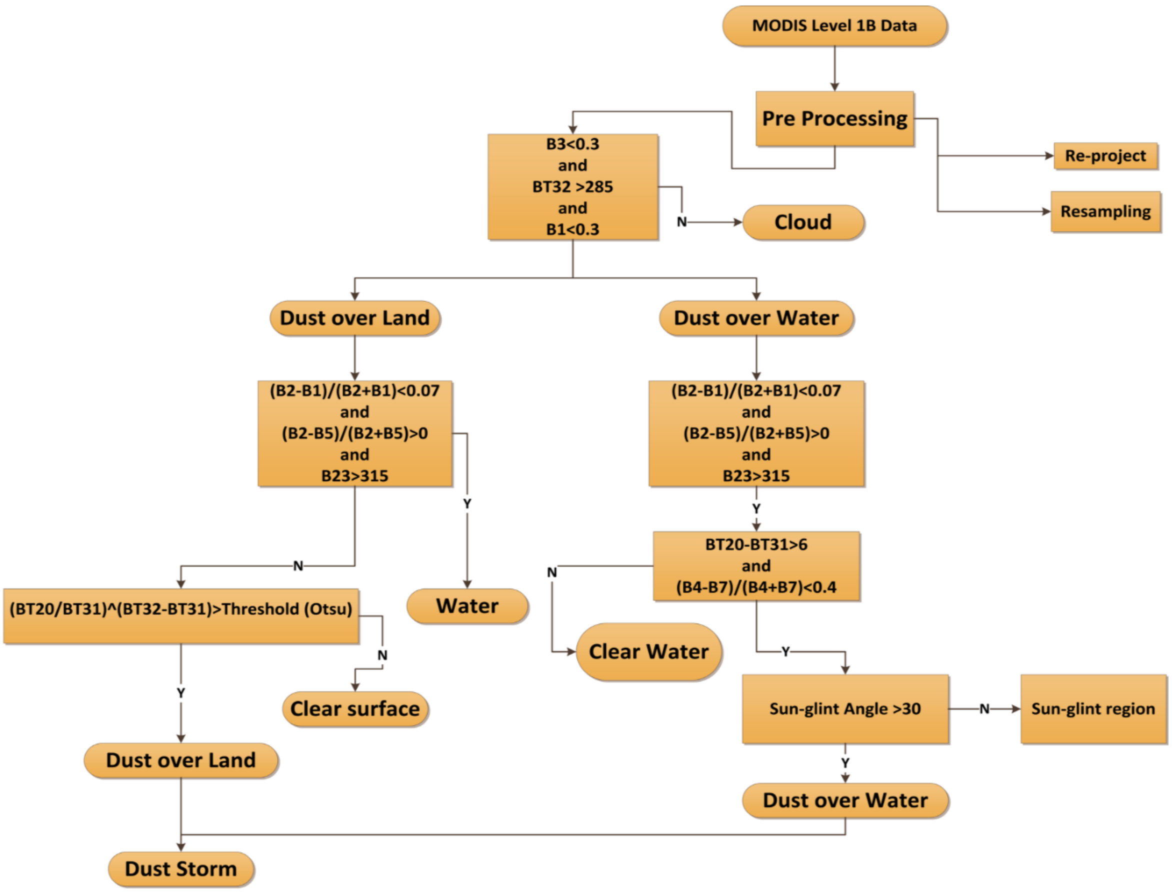

Fig. 3 The proposed dust detection approach.

2.3.1. Threshold estimation

Modeling of the spectral behavior of different objects was performed based on all the MODIS bands. Then, useful(valuable) bands were selected for each object. Approximately 10,000 pixels of each class in three images were sampled for five classes, and then, their statistical parameters were calculated. Fig. 4 represents the extracted spectral signatures of clouds, clear water, dust over water, desert, and dust over land.

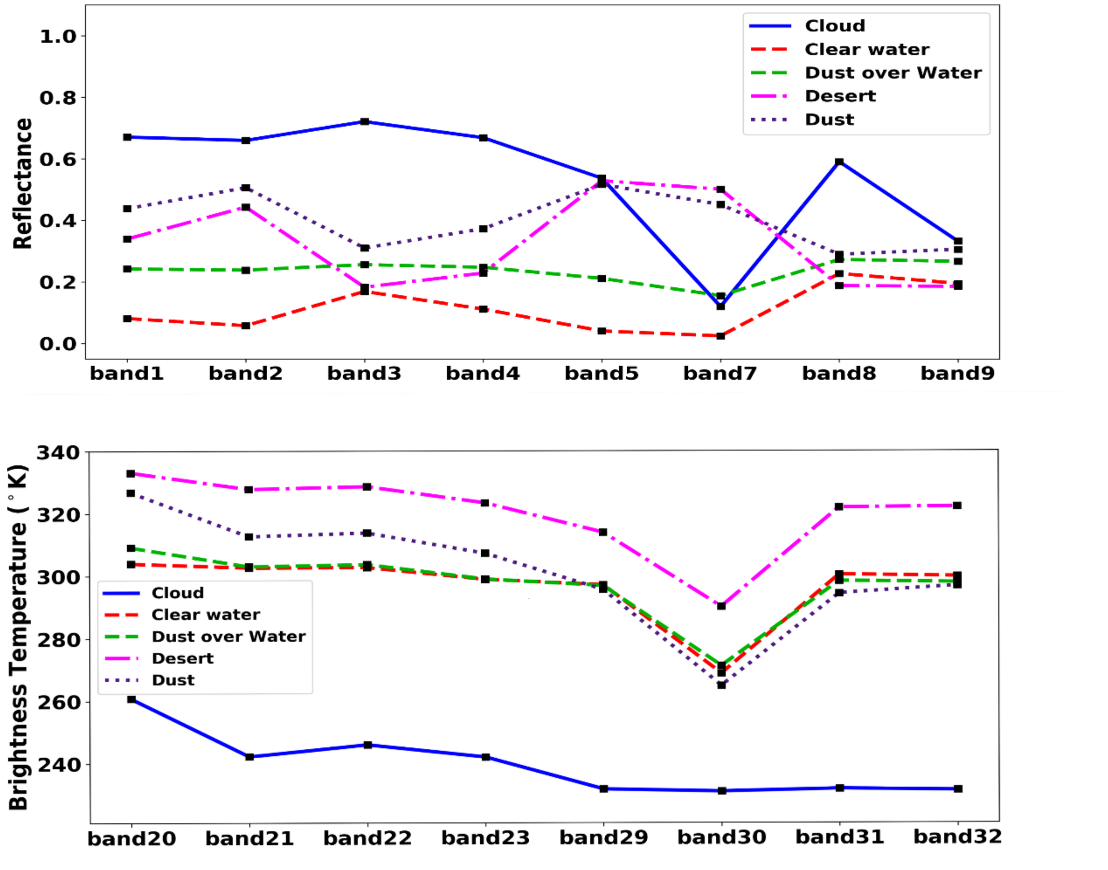

Fig. 4 Spectral Reflectance (top), and Brightness Temperature (bottom) signatures of different objects.

By calculating the statistical parameters and thresholds, the proposed indices were modeled and applied to the images. Fig. 5 shows the results in the box plots. A box plot displays the distribution of quantitative data so that it facilitates comparisons between variables. The box shows the quartiles of the distribution, and the whiskers show the rest of the dataset.

As is evident in Fig. 4-a, bands 1, 2, and 5 are suitable(becoming) bands for detecting water since they have a low reflection among the classes. One of the standard indices for identification and detection of water bodies is the Normalized difference water index (NDWI). Besides that, the Normalized difference vegetation index (NDVI) is suitable for finding water bodies that thin dust is present over water (Eq. (4) and (5)).

$$NDWI = \frac{R_{0.858\ \mu m} - R_{1.24\ \mu m}}{R_{0.858\ \mu m} + R_{1.24\ \mu m}} \tag{4}$$

$$NDVI = \frac{R_{0.858\ \mu m} - R_{0.645\ \mu m}}{R_{0.858\ \mu m} + R_{0.645\ \mu m}} \tag{5}$$

where $R_{0.645\ \mu m}$, $R_{0.858\ \mu m}$, and $R_{1.24\ \mu m}$ is the reflectance of band 1, 2, and 5.

Considering all datasets and bands, we noticed that the brightness temperature difference between band 20 and band 31, as well as a relationship between band 4 and band 7 is suitable to detect dust over water:

$$BTD_{3.7-11\ \mu m} = BT_{3.7\ \mu m} - BT_{11\ \mu m}\ , \tag{6}$$

$$R_{4,7} = \frac{R_{0.545\ \mu m} - R_{2.105\ \mu m}}{R_{0.545\ \mu m} + R_{2.105\ \mu m}} \tag{7}$$

where $R_{0.545\ \mu m}$ and $R_{2.105\ \mu m}$ are reflectance values in bands 4 and 7. $BT_{3.7\ \mu m}$ and $BT_{11\ \mu m}$ are the brightness temperature of bands 20 and 31.

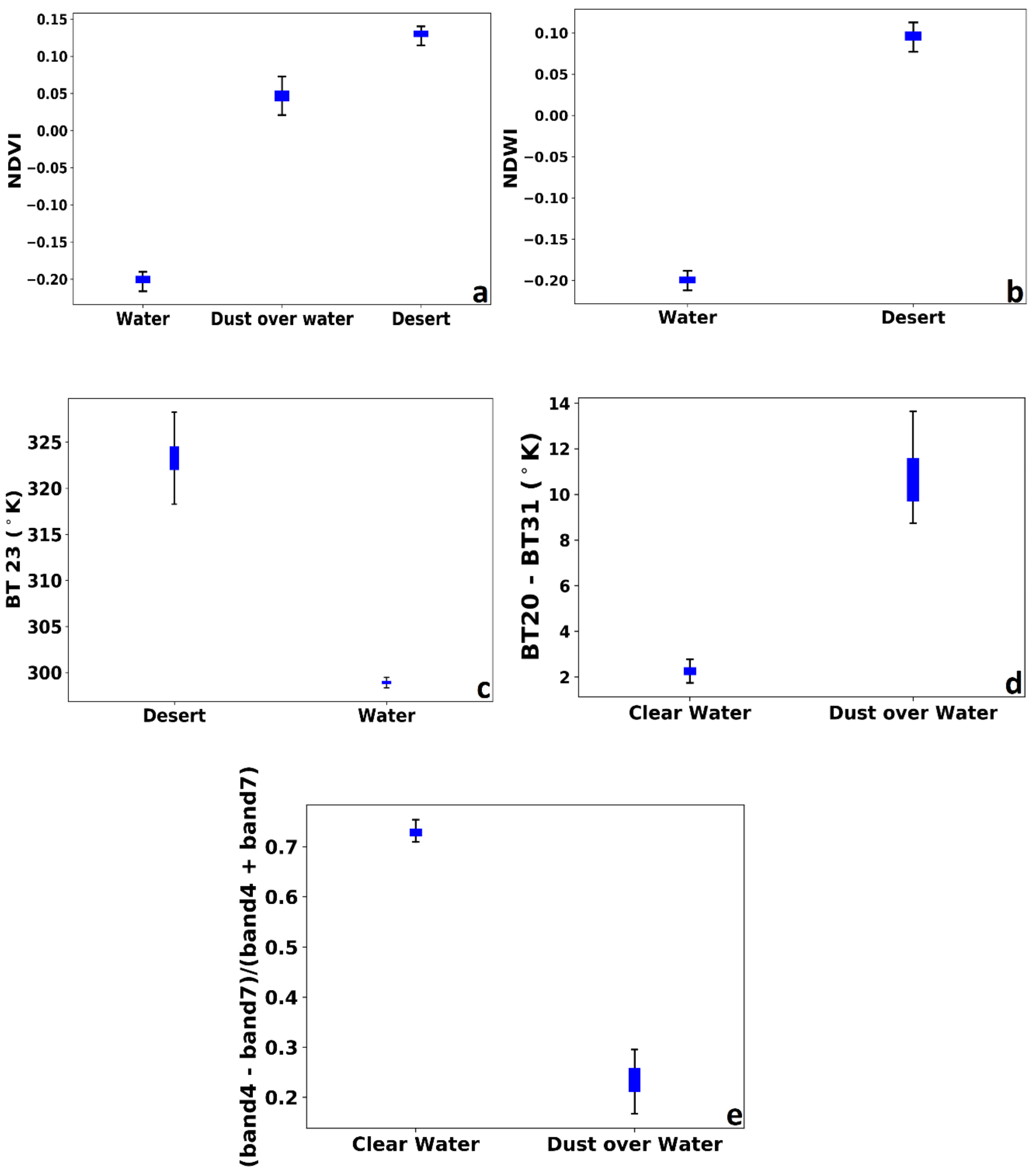

Fig. 5 Statistical analysis of a) NDVI of different phenomena, b) Normalized difference of band 4 and band 7, c) NDWI of different phenomena, d) Brightness temperature of band 23, and e) Brightness temperature difference of band 20 and band 31.

2.3.2. Clouds Masking

As shown in the flowchart (Fig. 3), the first step in implementing the proposed method is to mask clouds in the images. Clouds exhibit a much lower value of brightness temperature than other objects (Fig. 4-b). Brightness temperature is not capable of detecting thin clouds alone. Song et al. [65] suggested a method for mask clouds using reflection of band 1 (0.66 µm)-because of clouds' high reflection in this band-and brightness temperature of band 32 (12 µm). Unfortunately, after applying these formulas, clouds are not entirely masked, therefore, besides the mentioned bands, band 3 is utilized for cloud detection because of high reflection in this band (Fig. 4-a). Fig. 6-a depicts the result for the cloud mask of the proposed method on the image of the dust event in 2012.

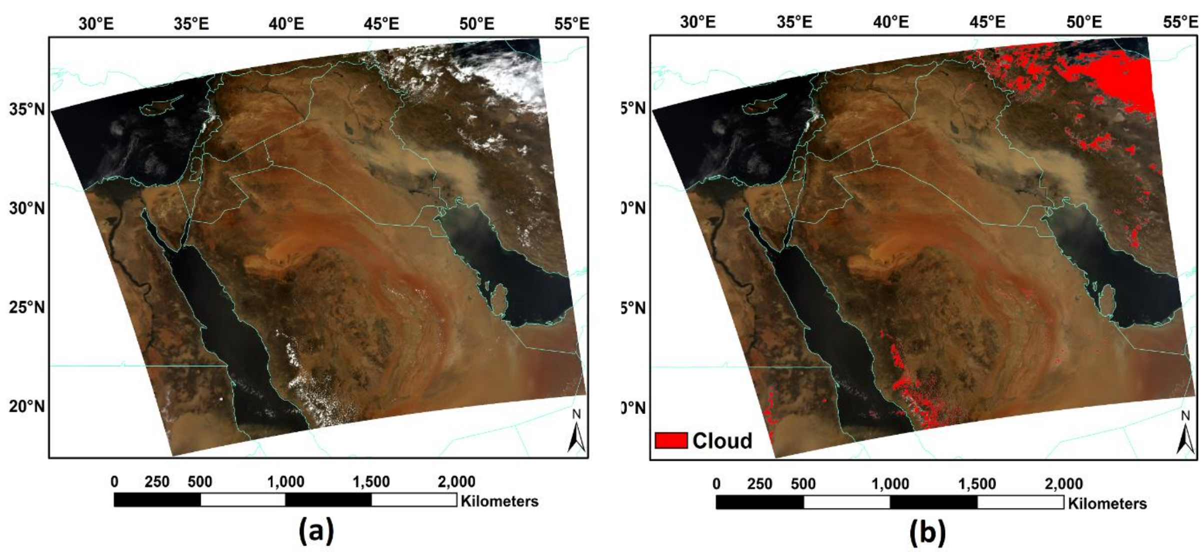

Fig. 6 Result of cloud masking (a), and the MODIS RGB image (b).

2.3.3. Water Delamination

The spectral behavior of thin dust over water differs from that of thick dust. Conventional strategies cannot detect thin dust over water. Accordingly, we mapped the water bodies in the image. Using spectral and statistical analysis, three formulas were selected for the identification of water bodies.

The amount of NDWI (Eq. (4)) to detect water is greater than zero (Fig. 5-c) [66, 67]. As well as, the value of NDVI (Eq. (5)) is less than zero, but According to Fig. 5-a, if thin dust was presented above the water bodies, the value of NDVI will be slightly higher than zero accordingly. Therefore, the threshold is set to a value above zero. Moreover, the brightness temperature of band 23 was used to detect water bodies with respect to the difference in value with other objects (Fig. 4-b and Fig. 5-d).

Fig. 7-a showed the results for the water bodies' delamination of the proposed method implemented on the image of the dust event in 2012.

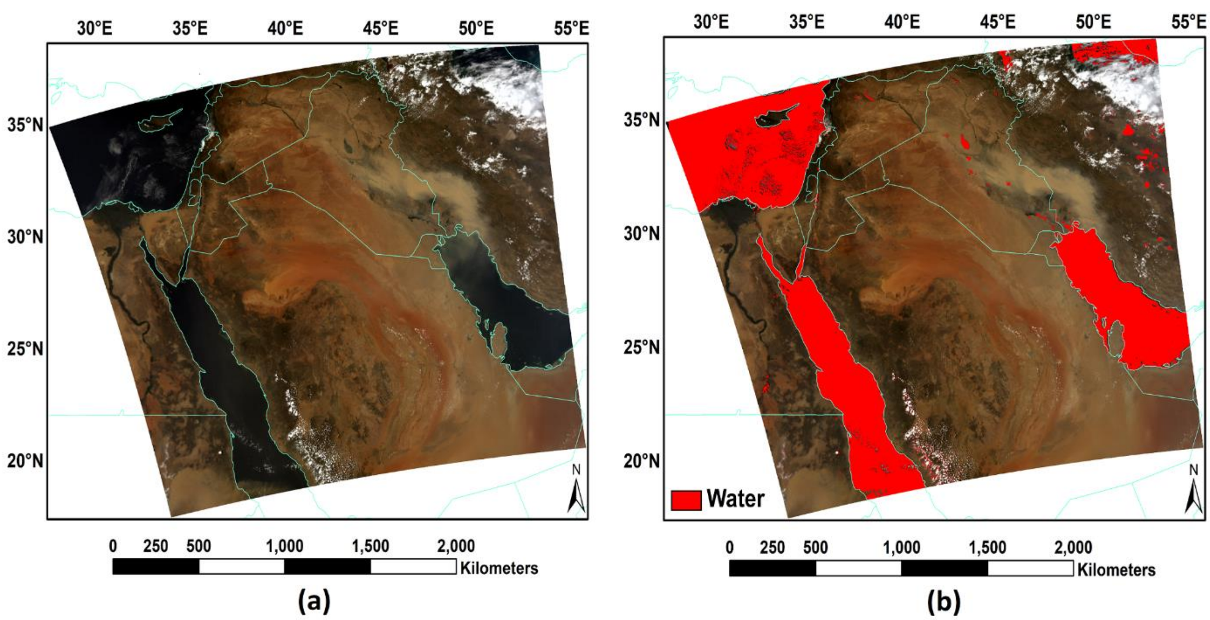

Fig. 7 Result of water delamination (a), and the MODIS RGB image (b).

2.3.4. Dust detection over the water surface

As mentioned earlier, the detection of thin dust over the water was one of the problems with previous algorithms. Therefore, to detect dust over water, first, we have to extract the water bodies. After identifying the water pixels in the image, we developed a method to distinguish between transparent and opaque water pixels. Considering the statistical analysis of the transparent and opaque water pixels, $BTD_{3.7\text{-}11\ \mu m}$ and $R_{4,7}$ (Eq. (6) and (7)) were applied to distinguish these two classes. MODIS Aqua and Terra images have sun-glint over water. In order to remove this effect, we detect dust for the sun-glint free region (with a sun-glint angle greater than 30 degrees) [68].

2.3.5. Dust detection over the land surface

The main challenge in detecting dust using satellite data is the separation of the spectral signal of dust from the surface of the Earth and the cloud, and this is especially challenging for bright surfaces [41, 42]. Due to similar reflectivity of dust particles and deserts in the visible bands, dust storm detection in the Middle East region is more complicated. Furthermore, using a single thermal band cannot distinguish between dust and other objects. As a solution to these limitations, using a combination of thermal, visible, and infrared bands from MODIS imagery can efficiently detect the dust [44, 24].

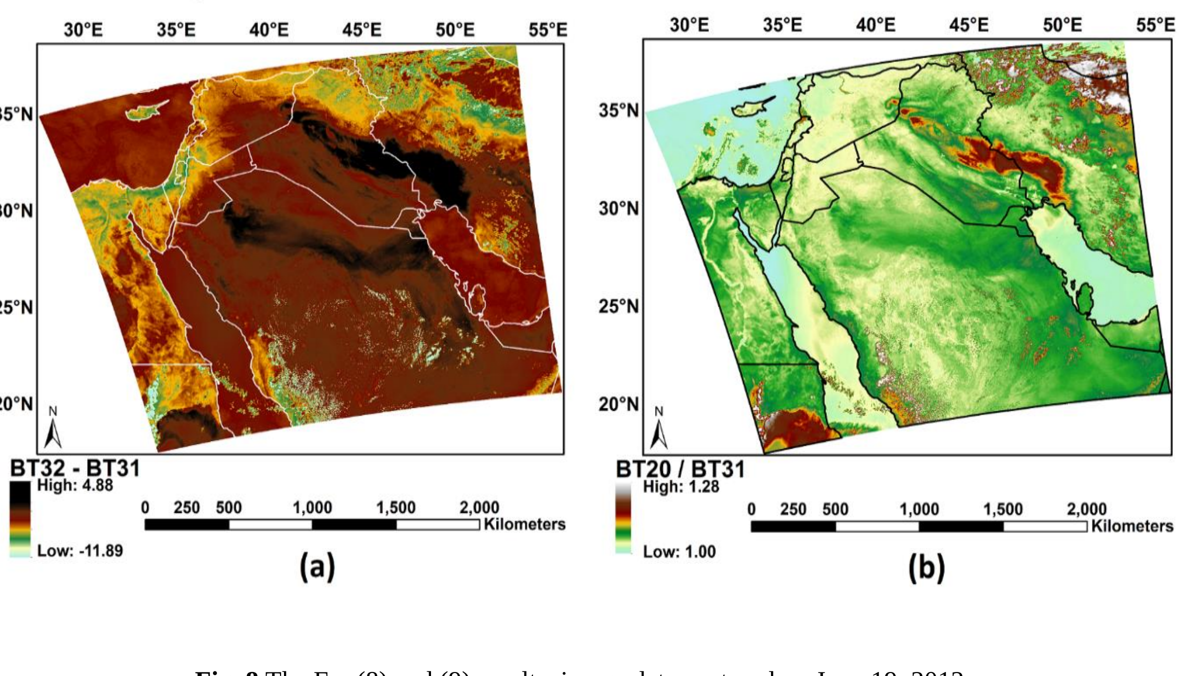

Fig. 8 The Eq. (8) and (9) results; image data captured on June 19, 2012.

Ackerman [43, 44] used the brightness temperature difference of band 20 (3.66-3.84 µm) and band 31 (11.28 – 1.78 µm), i.e., BTD $_{3.75\text{-}11\ \mu m}$, and difference of band 32 (12.22 – 11.77 µm) and band 31, i.e., BTD$_{12\text{-}11\ \mu m}$. Although BTD $_{3.75\text{-}11\ \mu m}$ can efficiently make a distinction between dust and ground surface, it cannot discriminate cloud and dust [44].

Based on the analysis of different bands, as well as the statistical analysis of different classes, we found that the brightness temperature of bands 20, 31, and 32 is suitable for dust detection over the land surfaces. These bands have been used in various studies to detect dust [43, 44]. For this reason, we have found two relationships to detect dust on land cover areas (Eq. (8) and (9)).

$$Band\ Ratio_{3.7\mu m-11\mu m} = \frac{\mathrm{BT}_{3.7\ \mu\mathrm{m}}}{\mathrm{BT}_{11\ \mu\mathrm{m}}} \tag{8}$$

$$\mathrm{BTD}_{11-12} = \mathrm{BT}_{11\ \mu\mathrm{m}} - \mathrm{BT}_{12\ \mu\mathrm{m}} \tag{9}$$

where BT$_{3.7\ \mu m}$, BT$_{11\ \mu m}$ and BT$_{12\ \mu m}$ are the brightness temperature of band 20, 31, and 32.

The 2012's satellite image was selected to perform this analysis. The results of these two equations are shown in Fig. 8-a and Fig. 8-b. Using these two equations separately, we cannot extract dust entirely from the image. For this reason, training regions were used to analyse these equations. Sampling was performed on thin and thick dust and different parts of the land, including bright and dark surface. More than 8000 pixels of land objects and about 1800 pixels of dust were selected. Sampling results showed that by combining the above two equations, dust over land could be well detected. Using these surveys, we found a relationship for dust detection (Eq. (10)).

$$\text{Improved Dust Index} = \left(\frac{BT_{3.7\,\mu m}}{BT_{11\,\mu m}}\right)^{(BT_{12\,\mu m} - BT_{11\,\mu m})} \tag{10}$$

The threshold for this index was calculated using the Otsu algorithm [69]. This algorithm is based on an iterating procedure through all the possible thresholds. It calculates a measure of spread on each side of the threshold and ultimately finds the optimal threshold values with the minimum inter- or the maximum intera- class variance. The dust index (Eq. (10)) was applied to the dust event images, and the result was classified into three classes of dust, land, and cloud (Fig. 9). The two threshold values (T1 and T2) are generally not constant and vary based on the season of occurring dust storms.

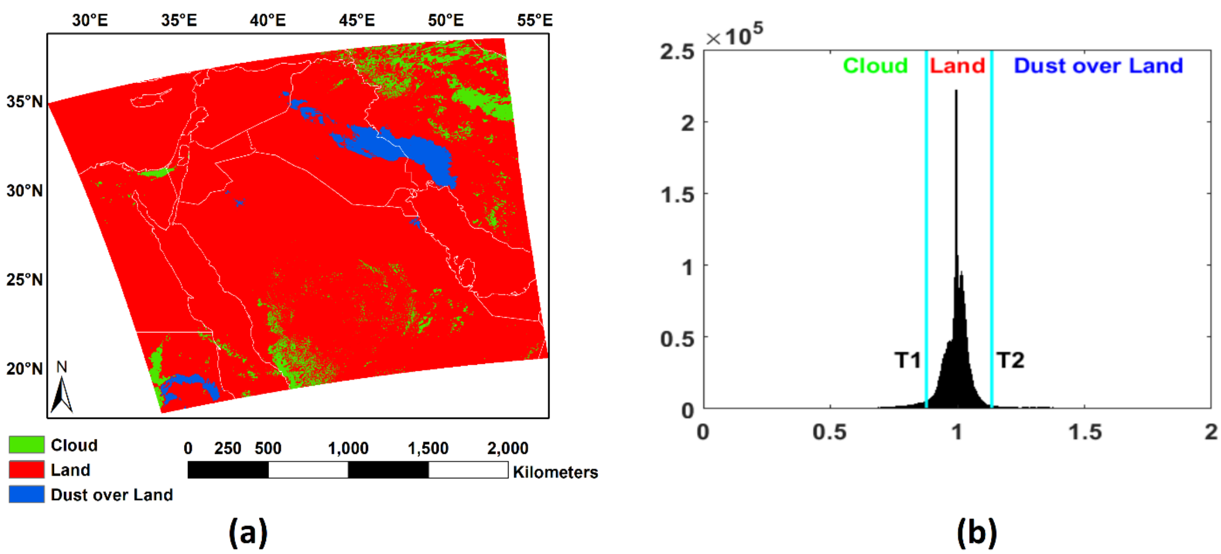

Fig. 9 Result of classification of the improved index with Otsu's thresholding (a), and the histogram of the image (b).

3. Results and Discussion

The proposed algorithm was applied and evaluated on ten dust occurrences from 2008 to 2018. Fig. 10-b, Fig. 11-b, and Fig. 12-b show the results of the proposed algorithm implementation on test images. In Fig. 10-b, it is apparent that the clouds masked well. Although there are many clouds in this image, the algorithm has been able to detect dust with decent accuracy. Thin dust over the water was also detected well. In the 2011 dust event, the algorithm has detected many dust particles over the water. The clouds are relatively well masked in the image (Fig. 11-b). In the 2012 dust event, water bodies were identified well, and thin and thick dust over them was detected with reasonable accuracy. Clouds were masked well. Finally, dust over the land was detected (Fig. 12-b).

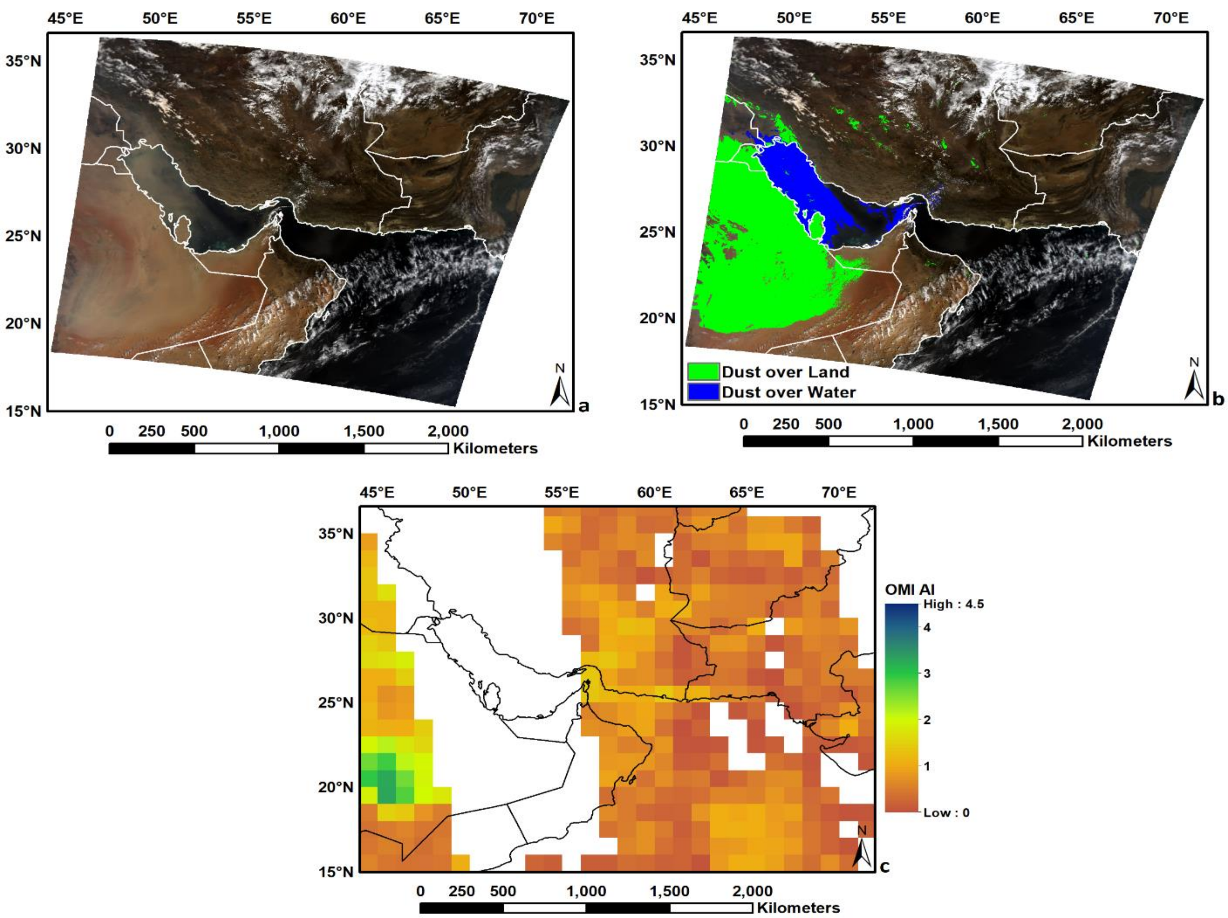

Fig. 10 Results of the proposed algorithm (a), MODIS RGB images (b), and OMI AI (c) obtained on March 5 2010.

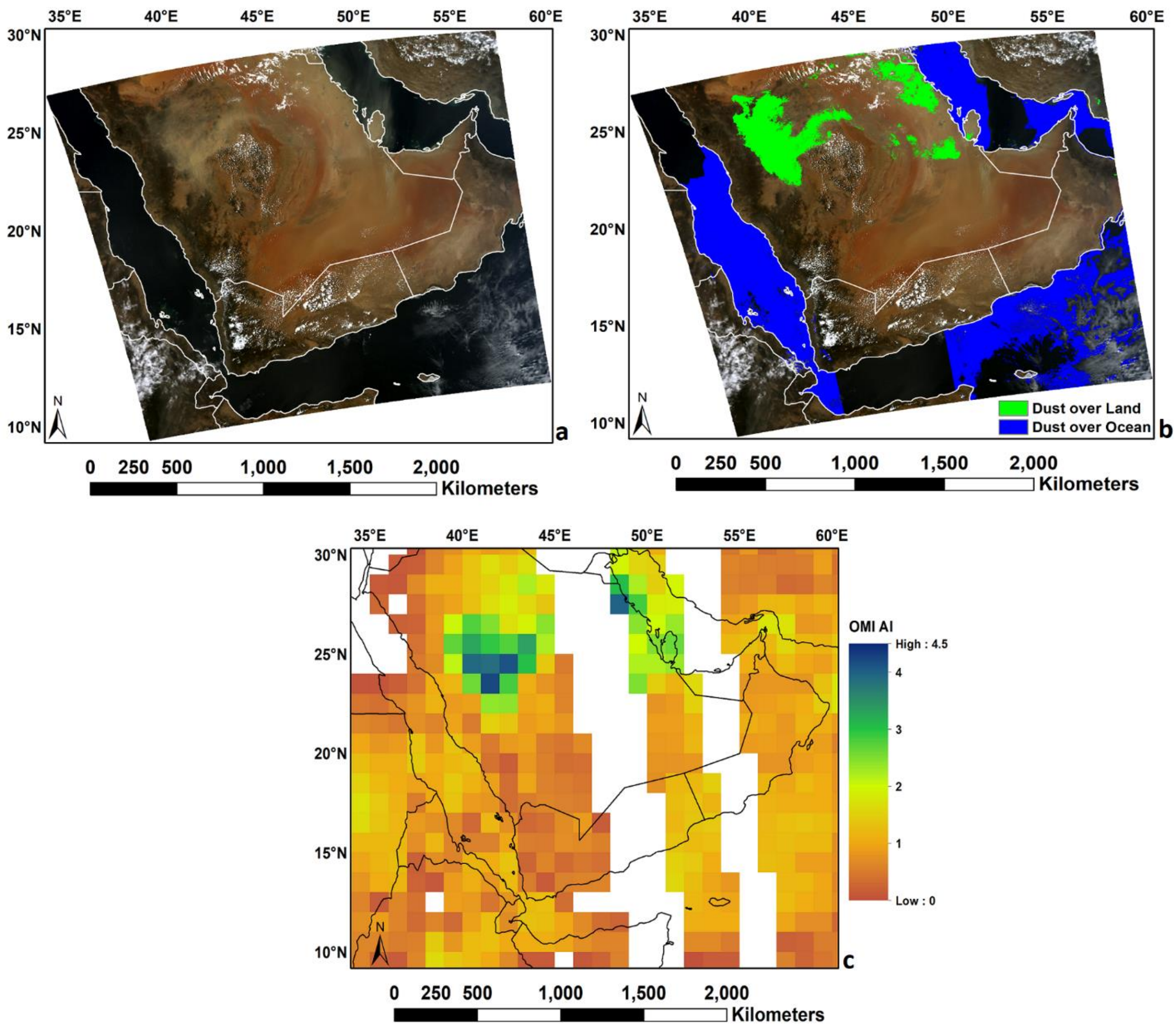

Fig. 11 Results of the proposed algorithm (a), MODIS RGB images (b), and OMI AI (c) obtained on June 3 2011.

Bin Abdulwahed, Dash and Roberts [5] evaluated various dust detection algorithms in the Middle East [5]. Their results showed that the Middle East Dust Index (MEDI) had difficulty distinguishing dust from dark and deserts regions. Also, their results showed that the brightness temperature difference is not capable of distinguishing dust from the bright surfaces well. They stated that the Normalized Difference Dust Index (NDDI) was more agree with the AERONET among the indicators they examined.

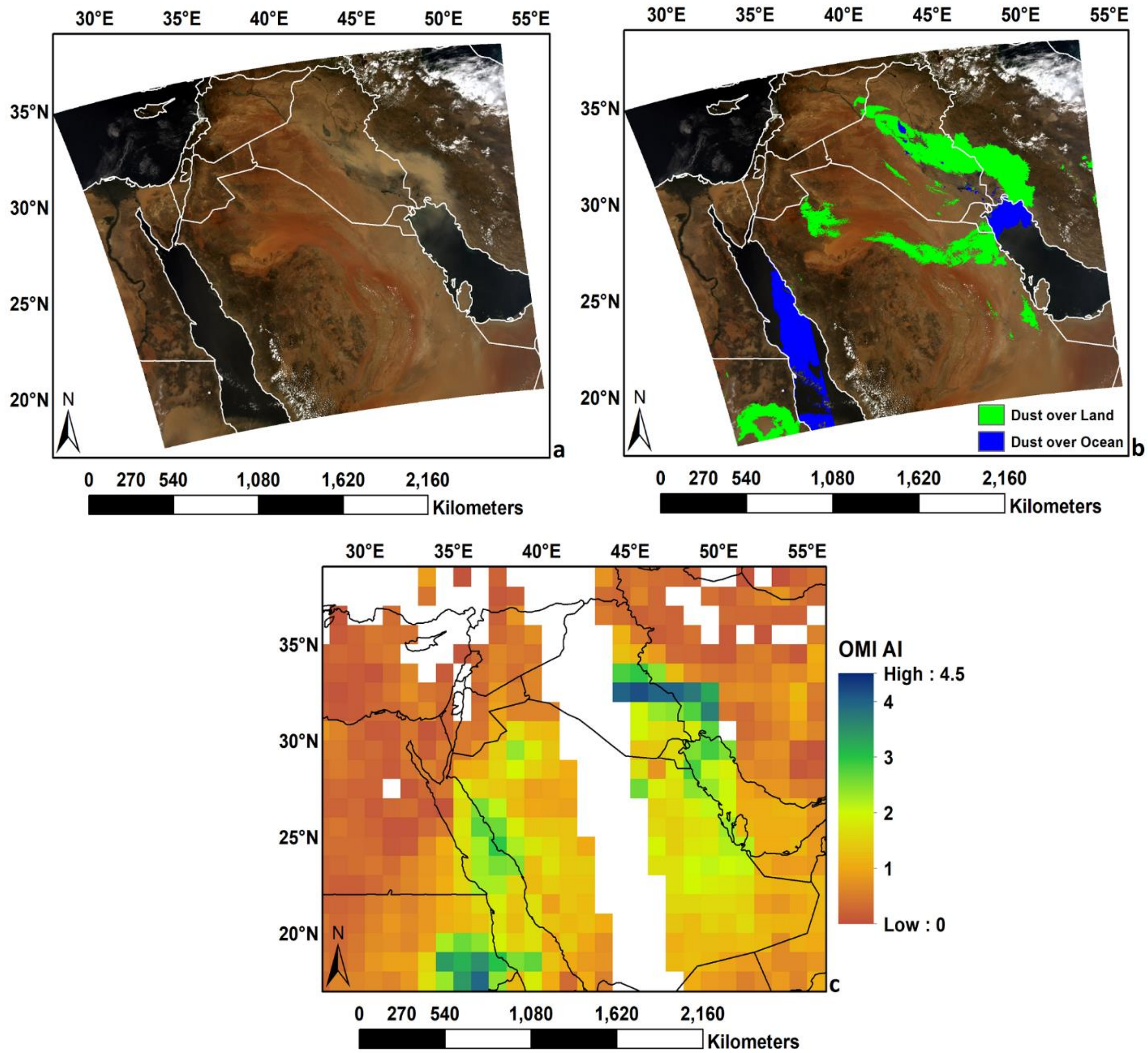

Fig. 12 Results of the proposed algorithm (a), MODIS RGB images (b), and OMI AI (c) obtained on June 19 2012.

Jafari and Malekian [61] also studied dust detection methods. They stated that available algorithms worked well in thick dust conditions, but in cloudy conditions, over water, and bright surfaces have different performance. As well as, they stated that examined algorithms generally misclassify thick clouds as dust.

Comparing the similar results from other research works, our results show that the clouds were relatively well masked in all images. The significant challenge for dust detection algorithms using the brightness temperature is to distinguish dusty pixels from the cloud. Because of the low spatial resolution of MODIS, thin clouds in pixels may have the same behavior of dust in the image. Appropriate cloud masking helped us to identify dust pixels better and might significantly reduce the number of false alarm pixels; in other words, pixels that were not dust but identified by the algorithm as dust. The next significant limitation of dust detection algorithms is the inability to detect dust over water bodies. It is challenging to identify thin dust pixels over water bodies with the brightness temperature merely. We need to detect thin dust over these areas with a separate method. Fortunately, in the proposed method, we were able to identify the dust smoothly by using statistical analysis.

Furthermore, distinguishing between dust pixels and bright surfaces such as deserts, which are abundant in the Middle East, is another challenge. Accurate threshold estimation in these areas is essential. We were able to overcome this problem to an acceptable level by automatically finding the threshold. Moreover, Lower threshold values in the improved index to detect dust over the land surface may cause problems between dust and desert. The proposed algorithm has a higher capability to distinguish between dust and other objects.

3.1. Validation

There are several ways to evaluate dust detection algorithms. In this paper, three separate panels were created to evaluate the proposed method for each three dust events. In each case, the results of the proposed method visually evaluated with MODIS RGB images where red, green, and blue are band 1, band 4, and band 3, respectively. Also, the results visually evaluated with OMI AI products. Although the OMI resolution is lower than the MODIS resolution, these products can indicate the intensity and location of the dust particles. Finally, the results of the method were evaluated with Iran synoptic data.

3.1.1. Visual evaluation of MODIS's dust detection

The results of the proposed algorithm are in good accordance with MODIS RGB images. Although MODIS images can be good at visually detecting thick dust, they have poor performance at detecting dust, especially in desert areas.

In the 2010 dust event, although the dust on the water and land is thin, the algorithm has been able to identify it relatively well (Fig. 10 a and b). However, a significantly lower threshold may be able to detect dust over the land more accurately. In the 2011 dust event, it is challenging to identify dust pixels over water and land visually. In this image, although the cloud is present in the image, the number of false alarms is near zero (Fig. 11 a and b). In the 2012 dust event, many south-western synoptic stations of IMO recorded a reduction in visibility to less than 1km. There is also some dust in the middle part of the image, but it cannot be seen in the RGB image (Fig. 12 a and b). There are some clouds in this image, but the number of false alarm pixels is deficient.

3.1.2. Visual companion with OMI-AI

OMI-AI for three dust events are presented in Fig. 10-c, Fig. 11-c, and Fig. 12-c. In the 2012 dust event, the results of the OMI-AI measurement are very consistent with the output of the proposed algorithm over water. An examination of the results of the proposed algorithm and images of OMI-AI shows that our method was able to perform better for the AI larger than 1.7. In the 2011 dust event, the results showed a good agreement between the proposed algorithm and OMI-AI over water and land.

Comparisons between the results of the proposed method and OMI-AI products showed that in Aqua images, due to the short time difference between Aqua and Aura satellite, the algorithm has been able to detect dust well. However, in the Terra satellite, due to the significant time difference, and the dynamic behavior of the dust, the results of the algorithm may be different from OMI.

3.1.3. Accuracy assessment

Because some of the synoptic stations were exterior of the studied region for dust detection, the analytical evaluation of the proposed algorithm was limited to the only overlapped areas. Horizontal visibility is a suitable parameter for the identification of the days that dust storms are occurred [26]. Therefore, 3-hourly synoptic data (i.e., horizontal visibility and code 06) records from 212 synoptic stations used to evaluate the proposed method. It should be noted that the maximum time difference between the MODIS images and the synoptic data was about 15 minutes.

For classification assessment, a confusion matrix is widely used to evaluate the performance of the algorithm. The confusion matrix, for a binary classification case, is a table with two rows and two columns. It reports the number of true positives (TP), true negatives (TN), false positives (FP), and false negatives (FN). For each of ten dust events, image pixels were classified into two classes of "dust" and "no dust." Here, TP represents the number of pixels where both synoptic data and proposed algorithm indicate the presence of "dust." FP is the number of pixels where synoptic data indicates "no dust." FN is the number of pixels where synoptic data indicates "dust," but the proposed algorithm indicates "no dust." Finally, the variable TN represents the number of pixels where both synoptic and proposed algorithms indicate "no dust."

Three statistical metrics, including accuracy, True Positive Rate (TPR), and False Discovery Rate (FDR), were calculated using the following equations and used for accuracy assessment.

$$\text{Accuracy} = \frac{TP + TN}{TP + FP + FN + TN} \tag{11}$$

$$\text{TPR} = \frac{TP}{TP + FN} \tag{12}$$

$$\text{FDR} = \frac{FP}{TP + FP} \tag{13}$$

The performance of the proposed algorithm is evaluated using contingency Table 3.

Table 3 The results of validation with synoptic data

Date	Accuracy	TPR	FDR
29 Oct 2017	0.76	0.74	0.30
05 Jul 2009	0.78	0.77	0.28
12 May 2018	0.77	0.76	0.28
31 Oct 2017	0.82	0.72	0.29
31 Oct 2017	0.81	0.73	0.29
19 Jun 2012	0.83	0.71	0.27
07 Jun 2008	0.81	0.78	0.31
Overall	0.80	0.74	0.29

As shown in Table 3, the overall accuracy for the dust detection algorithm was ~80 %. TPR and FDR were about 74 % and 29 %, respectively.

4. Conclusion

The real-time and automatic detection of dust, as a hazardous environmental phenomenon, is an essential and challenging application for different purposes. In this study, we proposed a method to detect and monitor the dust over water and land. This method was applied to daily MODIS

Level-1B data. The output dust maps were visually compared with MODIS RGB images and OMI-AI products as well as, the results of the proposed method were evaluated with observations from several synoptic ground stations of the Iranian meteorological organization. In total, three dust events were selected to collect sampling data and seven dust events to evaluate the efficiency of the proposed method. The overall accuracy of the dust detection algorithm was about 81%. The results showed that this model has acceptable accuracy for dust detection over both water and land areas. In particular, in contrast to the previous models, the proposed method was capable of detecting thin dust on the water. Low-density dust is not always visible in MODIS images due to its low spatial resolution. Therefore, there may be an uncertainty of detection over the corresponding areas. As a solution, higher spatial and temporal resolution satellite imagery can help better detection of dust in our future research. The proposed algorithm is planned to be implemented in the Google Earth Engine and to be served as the basis of a Spatial Support Decision System for various end-users.

References

1. L. San-Chao et al., “Detection of dust storms by using daytime and nighttime multi-spectral modis images,”*2006 IEEE International Symposium on Geoscience and Remote Sensing*,294-296,Ieee,2006),[doi:10.1109/igarss.2006.80].
2. A. S. Goudie and N. J. Middleton, *Desert dust in the global system*, Springer Science & Business Media, (2006), [doi:10.1007/3-540-32355-4].
3. H. M. El-Askary et al., ”A multisensor approach to dust storm monitoring over the nile delta,” *IEEE Transactions on Geoscience and Remote Sensing*, **41**, 10, 2386-2391, (2003), [doi:10.1109/tgrs.2003.817189].
4. M. F. Yassin, S. K. Almutairi and A. Al-Hemoud, ”Dust storms backward trajectories' and source identification over kuwait,” *Atmospheric research*, **212**, 158-171, (2018), [doi:10.1016/j.atmosres.2018.05.020].
5. A. Bin Abdulwahed, J. Dash and G. Roberts, ”An evaluation of satellite dust-detection algorithms in the middle east region,” *International journal of remote sensing*, **40**, 4, 1331-1356, (2019), [doi:10.1080/01431161.2018.1524589].
6. P. Jafary, A. Zandkarimi and M. Jannati, ”Annual monitoring of dust storm in iran and adjacent areas using modis images (1396 and 1397 hijri shamsi),” *International Archives*

of the Photogrammetry, Remote Sensing & Spatial Information Sciences, (2019), [doi:10.5194/isprs-archives-xlii-4-w18-565-2019].

7. M. Bennell, J. Leys and H. Cleugh, ”Sandblasting damage of narrow-leaf lupin (lupinus angustifolius l.): A field wind tunnel simulation,” *Soil Research*, **45**, 2, 119-128, (2007), [doi:10.1071/sr06066].
8. A. Chedin, V. Capelle and N. Scott, ”Detection of iasi dust aod trends over sahara: How many years of data required?,” *Atmospheric research*, **212**, 120-129, (2018), [doi:10.1016/j.atmosres.2018.05.004].
9. A. Al-Hemoud et al., ”Socioeconomic effect of dust storms in kuwait,” *Arabian Journal of Geosciences*, **10**, 1, 18, (2017), [doi:10.1007/s12517-016-2816-9].
10. T. X.-P. Zhao, S. Ackerman and W. Guo, ”Dust and smoke detection for multi-channel imagers,” *Remote Sensing*, **2**, 10, 2347-2368, (2010), [doi:10.3390/rs2102347].
11. P. Zhang et al., ”Identification and physical retrieval of dust storm using three modis thermal ir channels,” *Global and Planetary Change*, **52**, 1-4, 197-206, (2006), [doi:10.1016/j.gloplacha.2006.02.014].
12. H. El-Askary et al., “Introducing new approaches for dust storms detection using remote sensing technology,”*IGARSS 2003. 2003 IEEE International Geoscience and Remote Sensing Symposium. Proceedings (IEEE Cat. No. 03CH37477)*,2439-2441,IEEE,2003),[doi:10.1109/igarss.2003.1294468].
13. L. Perez et al., ”Saharan dust, particulate matter and cause-specific mortality: A case-crossover study in barcelona (spain),” *Environ Int*, **48**, 150-155, (2012), [doi:10.1016/j.envint.2012.07.001].
14. D. W. Griffin and C. A. Kellogg, ”Dust storms and their impact on ocean and human health: Dust in earth’s atmosphere,” *EcoHealth*, **1**, 3, 284-295, (2004), [doi:10.1007/s10393-004-0120-8].
15. B. Laurent et al., ”Simulation of the mineral dust emission frequencies from desert areas of china and mongolia using an aerodynamic roughness length map derived from the polder/adeos 1 surface products,” *Journal of Geophysical Research: Atmospheres*, **110**, D18, (2005), [doi:10.1029/2004jd005013].
16. A. Zandkarimi and P. Fatehi, ”Dust storm detection using modis data over the middle east,” *The International Archives of Photogrammetry, Remote Sensing and Spatial Information Sciences*, **42**, 1147-1151, (2019), [doi:10.5194/isprs-archives-xlii-4-w18-1147-2019].
17. M. H. Saeifar and B. Alijani, ”Detection of dust storm origins in the middle east by remotely sensed data,” *Journal of the Indian Society of Remote Sensing*, **47**, 11, 1883-1893, (2019), [doi:10.1007/s12524-019-01030-5].
18. Y. J. Kaufman, D. Tanre and O. Boucher, ”A satellite view of aerosols in the climate system,” *Nature*, **419**, 6903, 215-223, (2002), [doi:10.1038/nature01091].
19. F. Marchese et al., ”An enhanced satellite-based algorithm for detecting and tracking dust outbreaks by means of seviri data,” *Remote Sensing*, **9**, 6, 537, (2017), [doi:10.3390/rs9060537].
20. M. Akhlaq, T. R. Sheltami and H. T. Mouftah, ”A review of techniques and technologies for sand and dust storm detection,” *Reviews in Environmental Science and Bio/Technology*, **11**, 3, 305-322, (2012), [doi:10.1007/s11157-012-9282-y].
21. W. Emery and A. Camps, *Introduction to satellite remote sensing: Atmosphere, ocean, land and cryosphere applications*, Elsevier, (2017), [doi:10.1109/mgrs.2018.2873040].

22. K. Schepanski, I. Tegen and A. Macke, ”Comparison of satellite based observations of saharan dust source areas,” *Remote Sensing of Environment*, **123**, 90-97, (2012), [doi:10.1016/j.rse.2012.03.019].

23. H. El-Askary et al., ”Dust storms detection over the indo-gangetic basin using multi sensor data,” *Advances in Space Research*, **37**, 4, 728-733, (2006), [doi:10.1016/j.asr.2005.03.134].

24. T. Takashima and K. Masuda, ”Emissivities of quartz and sahara dust powders in the infrared region (7–17 μ),” *Remote Sensing of Environment*, **23**, 1, 51-63, (1987), [doi:10.1016/0034-4257(87)90070-8].

25. P. D. Kunte and M. Aswini, ”Detection and monitoring of super sandstorm and its impacts on arabian sea—remote sensing approach,” *Atmospheric Research*, **160**, 109-125, (2015), [doi:10.1016/j.atmosres.2015.03.003].

26. M. C. Baddock, J. E. Bullard and R. G. Bryant, ”Dust source identification using modis: A comparison of techniques applied to the lake eyre basin, australia,” *Remote Sensing of Environment*, **113**, 7, 1511-1528, (2009), [doi:10.1016/j.rse.2009.03.002].

27. M. J. Butt, M. E. Assiri and M. A. Ali, ”Assessment of aod variability over saudi arabia using modis deep blue products,” *Environmental pollution*, **231**, 143-153, (2017), [doi:10.1016/j.envpol.2017.07.104].

28. I. Gunaseelan, B. V. Bhaskar and K. Muthuchelian, ”The effect of aerosol optical depth on rainfall with reference to meteorology over metro cities in india,” *Environ Sci Pollut Res Int*, **21**, 13, 8188-8197, (2014), [doi:10.1007/s11356-014-2711-4].

29. S. Gehlot, P. J. Minnett and D. Stammer, ”Impact of sahara dust on solar radiation at cape verde islands derived from modis and surface measurements,” *Remote Sensing of Environment*, **166**, 154-162, (2015), [doi:10.1016/j.rse.2015.05.026].

30. S. S. Park et al., ”Combined dust detection algorithm by using modis infrared channels over east asia,” *Remote sensing of environment*, **141**, 24-39, (2014), [doi:10.1016/j.rse.2013.09.019].

31. S. Janugani et al., “Directional analysis and filtering for dust storm detection in noaa-avhrr imagery,”*Algorithms and Technologies for multispectral, hyperspectral, and ultraspectral imagery XV*,73341G,International Society for Optics and Photonics,2009),[doi:10.1117/12.819070].

32. A. T. Evan, A. K. Heidinger and M. J. Pavolonis, ”Development of a new over-water advanced very high resolution radiometer dust detection algorithm,” *International Journal of Remote Sensing*, **27**, 18, 3903-3924, (2006), [doi:10.1080/01431160600646359].

33. M. Rezaei et al., ”Analysis of spatio-temporal dust aerosol frequency over iran based on satellite data,” *Atmospheric Pollution Research*, **10**, 2, 508-519, (2019), [doi:10.1016/j.apr.2018.10.002].

34. Y. Yang et al., ”A simplified suomi npp viirs dust detection algorithm,” *Journal of Atmospheric and Solar-Terrestrial Physics*, **164**, 314-323, (2017), [doi:10.5270/esa-91oxxtk].

35. P. Alpert et al., ”Vertical distribution of saharan dust based on 2.5-year model predictions,” *Atmospheric Research*, **70**, 2, 109-130, (2004), [doi:10.1016/j.atmosres.2003.11.001].

36. B. Chen et al., ”Detection of dust aerosol by combining calipso active lidar and passive iir measurements,” *Atmospheric Chemistry & Physics Discussions*, **10**, 2, (2010), [doi:10.5194/acp-10-4241-2010].

37. A. Moridnejad, N. Karimi and P. A. Ariya, ”A new inventory for middle east dust source points,” *Environ Monit Assess*, **187**, 9, 582, (2015), [doi:10.1007/s10661-015-4806-x].

38. Y. J. Kaufman et al., ”The effect of smoke, dust, and pollution aerosol on shallow cloud development over the atlantic ocean,” *Proc Natl Acad Sci U S A*, **102**, 32, 11207-11212, (2005), [doi:10.1073/pnas.0505191102].

39. D. Tanré et al., ”Remote sensing of aerosol properties over oceans using the modis/eos spectral radiances,” *Journal of Geophysical Research: Atmospheres*, **102**, D14, 16971-16988, (1997), [doi:10.1029/96jd03437].

40. A. Sayer et al., ”Validation and uncertainty estimates for modis collection 6 “deep blue” aerosol data,” *Journal of Geophysical Research: Atmospheres*, **118**, 14, 7864-7872, (2013), [doi:10.1002/jgrd.50600].

41. N. C. Hsu et al., ”Deep blue retrievals of asian aerosol properties during ace-asia,” *IEEE Transactions on Geoscience and Remote Sensing*, **44**, 11, 3180-3195, (2006), [doi:10.1109/tgrs.2006.879540].

42. N. C. Hsu et al., ”Aerosol properties over bright-reflecting source regions,” *IEEE Transactions on Geoscience and Remote Sensing*, **42**, 3, 557-569, (2004), [doi:10.1016/s0021-8502(98)90762-5].

43. S. A. Ackerman, ”Remote sensing aerosols using satellite infrared observations,” *Journal of Geophysical Research: Atmospheres*, **102**, D14, 17069-17079, (1997), [doi:10.1029/96jd03066].

44. ---, ”Using the radiative temperature difference at 3.7 and 11 μm to tract dust outbreaks,” *Remote Sensing of Environment*, **27**, 2, 129-133, (1989), [doi:10.1016/0034-4257(89)90012-6].

45. H. Yue et al., ”The brightness temperature adjusted dust index: An improved approach to detect dust storms using modis imagery,” *International journal of applied earth observation and geoinformation*, **57**, 166-176, (2017), [doi:10.1016/j.jag.2016.12.016].

46. X. Hao and J. J. Qu, ”Saharan dust storm detection using moderate resolution imaging spectroradiometer thermal infrared bands,” *Journal of Applied Remote Sensing*, **1**, 1, 013510, (2007), [doi:10.1117/1.2740039].

47. N. Karimi et al., ”Comparison of dust source identification techniques over land in the middle east region using modis data,” *Canadian Journal of Remote Sensing*, **38**, 5, 586-599, (2012), [doi:10.5589/m12-048].

48. Y. Liu and R. Liu, “A thermal index from modis data for dust detection,”*2011 IEEE International Geoscience and Remote Sensing Symposium*,3783-3786,IEEE,2011),[doi:10.1109/igarss.2011.6050054].

49. J. Singh et al., ”Dust detection and aerosol properties over arabian sea using modis data,” *Earth Systems and Environment*, **3**, 1, 139-152, (2019), [doi:10.1007/s41748-018-0079-1].

50. J. J. Qu et al., ”Asian dust storm monitoring combining terra and aqua modis srb measurements,” *IEEE Geoscience and remote sensing letters*, **3**, 4, 484-486, (2006), [doi:10.1109/lgrs.2006.877752].

51. J. Roskovensky et al., ”Simultaneous retrieval of aerosol and thin cirrus optical depths using modis airborne simulator data during crystal-face and clams,” *Geophysical research letters*, **31**, 18, (2004), [doi:10.1029/2004gl020457].

52. M. Samadi et al., ”Global dust detection index (gddi); a new remotely sensed methodology for dust storms detection,” *J Environ Health Sci Eng*, **12**, 1, 20, (2014), [doi:10.1186/2052-336X-12-20].

53. S. Miller, ”A consolidated technique for enhancing desert dust storms with modis,” *Geophysical Research Letters*, **30**, 20, (2003), [doi:0.1029/2003gl018279].
54. E. El-ossta, R. Qahwaji and S. S. Ipson, ”Detection of dust storms using modis reflective and emissive bands,” *IEEE Journal of Selected Topics in Applied Earth Observations and Remote Sensing*, **6**, 6, 2480-2485, (2013), [doi:10.1109/jstars.2013.2248131].
55. S. Albugami et al., ”Evaluating modis dust-detection indices over the arabian peninsula,” *Remote Sensing*, **10**, 12, 1993, (2018), [doi:10.3390/rs10121993].
56. M. Boroughani et al., ”Application of remote sensing techniques and machine learning algorithms in dust source detection and dust source susceptibility mapping,” *Ecological Informatics*, **56**, 101059, (2020), [doi:10.1016/j.ecoinf.2020.101059].
57. P. Ginoux et al., ”Global-scale attribution of anthropogenic and natural dust sources and their emission rates based on modis deep blue aerosol products,” *Reviews of Geophysics*, **50**, 3, (2012), [doi:10.1029/2012rg000388].
58. F. Khoshakhlagh, M. Najafi and M. Samadi, ”An analysis on synoptic patterns of springtime dust occurrence in west of iran,” (2012), [doi:10.1256/qj.05.109].
59. H. K. H. Furman, ”Dust storms in the middle east: Sources of origin and their temporal characteristics,” *Indoor and Built Environment*, **12**, 6, 419-426, (2003), [doi:10.1177/1420326x03037110].
60. L. Han et al., ”An enhanced dust index for asian dust detection with modis images,” *International journal of remote sensing*, **34**, 19, 6484-6495, (2013), [doi:10.1080/01431161.2013.802055].
61. R. Jafari and M. Malekian, ”Comparison and evaluation of dust detection algorithms using modis aqua/terra level 1b data and modis/omi dust products in the middle east,” *International Journal of Remote Sensing*, **36**, 2, 597-617, (2015), [doi:10.1080/01431161.2014.999880].
62. K. Sun, Q. Su and Y. Ming, ”Dust storm remote sensing monitoring supported by modis land surface reflectance database,” *Remote Sensing*, **11**, 15, 1772, (2019), [doi:10.3390/rs11151772].
63. D. Kaskaoutis et al., ”The aura–omi aerosol index distribution over greece,” *Atmospheric Research*, **98**, 1, 28-39, (2010), [doi:10.1109/igarss.2011.6050054].
64. O. Torres et al., ”Aerosols and surface uv products from ozone monitoring instrument observations: An overview,” **112**, D24, (2007),
65. X. Song, Z. Liu and Y. Zhao, “Cloud detection and analysis of modis image,”*IGARSS 2004. 2004 IEEE International Geoscience and Remote Sensing Symposium*,2764-2767,IEEE,2004),[doi:10.1029/2004jd005013].
66. H. J. I. j. o. r. s. Xu, ”Modification of normalised difference water index (ndwi) to enhance open water features in remotely sensed imagery,” **27**, 14, 3025-3033, (2006),
67. S. K. J. I. j. o. r. s. McFeeters, ”The use of the normalized difference water index (ndwi) in the delineation of open water features,” **17**, 7, 1425-1432, (1996),
68. P. Ciren and S. J. J. o. G. R. A. Kondragunta, ”Dust aerosol index (dai) algorithm for modis,” **119**, 8, 4770-4792, (2014),
69. N. J. I. t. o. s. Otsu, man, and cybernetics, ”A threshold selection method from gray-level histograms,” **9**, 1, 62-66, (1979),